

# Universal spatial inflation of human mobility

Lu Zhong<sup>1,2,6</sup>, Lei Dong<sup>3,6</sup>, Qi Wang<sup>4</sup>, Chaoming Song<sup>5</sup>, Jianxi Gao<sup>1,2\*</sup>

<sup>1</sup>*Department of Computer Science, Rensselaer Polytechnic Institute, Troy, NY, USA*

<sup>2</sup>*Network Science and Technology Center, Rensselaer Polytechnic Institute, Troy, NY, USA*

<sup>3</sup>*Institute of Remote Sensing and Geographical Information Systems, School of Earth and Space Sciences, Peking University, Beijing, China*

<sup>4</sup>*Department of Civil and Environmental Engineering, Northeastern University, Boston, MA, USA*

<sup>5</sup>*Department of Physics, University of Miami, Coral Gables, FL, USA*

<sup>6</sup>*These authors contributed equally: Lu Zhong, Lei Dong.*

*Email: gaoj8@rpi.edu*

**Human mobility patterns reflect our interactions with the environment. While extensive research has focused on specific spatial scales—such as intracity or intercity—universal mobility characteristics across various scales remain largely unexplored. Here, by partitioning trajectories into modules through network community detection, we find that the geospatial extent of modules increases sublinearly with distance from home, indicating a universal inflation law that holds across three orders of magnitude and is independent of demographic factors. Our further investigation highlights a potential connection between this inflation law and hierarchical urban structure. These findings deepen our understanding of human mobility dynamics, with implications for urban planning, tourism management, and epidemic intervention.**

In human societies, the vibrant and varied movement of individuals plays a crucial role in nearly all facets of socioeconomic life—from social connections to disease transmission—and is essential to the development of infrastructure and amenities<sup>1-3</sup>. As a mobile species, human movement in many ways resembles the Lévy flight of animals in the natural world<sup>4,5</sup>. A key difference, however, is that the geographic space of human activity presents an organized hierarchy that has multiple spatial scales<sup>6-8</sup>, ranging from neighborhoods to cities, and extending to states and countries. Yet, current analyses of human movement typically focus on specific spatial scales (see Table S1). For instance, the radiation model is used to capture intercity migration<sup>9</sup>, while the visitation law governs intracity mobility<sup>10</sup>. Some models, such as the gravity model, are relatively robust at different scales, but in practice, they are often calibrated at a specific scale<sup>1,2</sup>. This focus limits our understanding of mobility across different geographic scales. A major reason for this limitation is the reliance on predetermined spatial scales, such as grid cells or administrative divisions, in data analysis and modeling. Here, we introduce a network-based approach to representing individual mobility trajectories that allows for the effective extraction of structural patterns across different spatial scales without predefined units.

Our analysis is based on high-resolution cell phone datasets from three countries with diverse cultural and developmental contexts (Figs. S1 and Table S2). The first dataset encompasses six months of privacy-enhanced global positioning system trajectories from two million anonymous users in the United States (U.S.). The second and third datasets consist of two weeks of call detail records (CDR) from 300,000 anonymous users in Senegal and 50,000 anonymous users in Ivory Coast, respectively. We construct a network for each user's trajectory, representing stay points

as network nodes and the trips between consecutive stay points as edges (Fig. 1a-b). In this network, the weight of edges is determined by the reciprocal of the spatial distance between these stay points, reflecting inverse distance weighting principles in spatial analysis<sup>11</sup>. This means that shorter spatial distances yield larger edge weights (see Method).

We apply the Louvain method<sup>12</sup> to partition trajectory networks into multiple modules and examine the correlation between module characteristics and their distance from the user’s home (Methods, Figs. S2-S6). We focus on distance from home because numerous studies have shown that home location serves as a critical anchor in shaping human mobility patterns<sup>13,14</sup>. Figure 1b illustrates a user’s trajectory partitioned into five modules based on spatial and topological proximity. For each module, we measure its spatial size  $r_c$  (the average distance of stay points to the module centroid) and the distance from its centroid to the home location  $d_c$ . As demonstrated by the three sample users in Fig. 1c, the radius of the module increases with distance from home. Our thorough analysis of all trajectories reveals a remarkably universal pattern:

$$r_c \sim d_c^\kappa, \tag{1}$$

where  $\kappa$  is approximately  $0.61 \pm 0.3$  for US data across the West, Northeast, Midwest, and South regions (Fig. 1d-g), with  $\kappa$  around 0.58 for Senegal (Fig. 1h) and 0.58 for Ivory Coast (Fig. 1i). We refer to this pattern in human mobility as the “*inflation law*” – as individuals move farther from home, their exploration scope (module sizes) increases sub-linearly. Specifically, when travel distances increase from  $10km$ ,  $100km$ , and  $1000km$ , the module radius expands to  $4km$ ,  $15km$ , and  $63km$ , corresponding to neighborhood, city, and state scales.

To verify the generality of this inflation pattern, we conducted robustness checks on module size measurement, module extraction methods, data sampling ratio, and demographic factors (Figs. S6-S14). We quantified module size using the convex hull of visited locations within each module (Fig. S6) and applied alternative partitioning methods for module extraction in trajectory networks (Fig. S7). Furthermore, we estimated Eq. (1) for each U.S. state (Fig. S9–S10) and categorized users based on demographic attributes such as age, gender, race, poverty level, household income, and home location (Fig. S11). The results demonstrate that the inflation law is robust across datasets from different regions and remains consistent under varying measures of spatial module extent, extraction methods, and diverse demographic groups.

To further explore the inflation law, we examine the geographic distribution of individual modules within the hierarchically interconnected urban system<sup>3,7</sup>, which naturally results in a power-law relationship between the level of each unit and its size, as exemplified by central place theory<sup>7</sup>. However, due to varying standards of administrative divisions across countries, directly comparing hierarchical levels based on administrative divisions is challenging. To address this, we establish a consistent spatial hierarchy across regions by defining hierarchical levels  $L$  using the H3 geospatial indexing system<sup>15</sup>. Specifically, we compute the movement matrix between H3 cells at each resolution and apply a community detection algorithm to aggregate cells, thereby defining the level units at each resolution (see Methods). Figure 2a shows the resultant hierarchical partition of Boston, Massachusetts, where lower-level units cover small areas (e.g., neighborhoods), while higher-level units cover larger areas (e.g., cities and regions) and encompass lower-level units and their interconnections.

As shown in Fig. 2b-c, in the destination Boston, Massachusetts, module networks farther from home (e.g., 10km, 100km, 1000km) typically involve travel across higher spatial levels. To analyze this, we match the individual module network to spatial units at different hierarchical levels and assign modules to levels  $L_c$  if their area overlap exceeds 80% (see Methods). Analysis of all three countries' datasets demonstrates that module levels and their distance from home can be well-fitted by the relationship  $L_c \sim \log(d_c)$  (Fig. 2d). Additionally, as shown in Fig. 2e, the size  $R$  of a spatial unit and its corresponding hierarchical level following  $\log(R) \sim L$ . Combining these findings, we establish that the module follows  $\log(R) \sim \log(d_c)$ . We further use the administrative hierarchy defined by the U.S. Census Bureau (county division, county, state, region) to perform a robustness check. As depicted in Fig. S15, the spatial size increases with the administrative level, adhering to the same relationship observed with the H3 delineation, and module levels increase with distance from home. In both our defined hierarchy and the administrative hierarchy, mobility modules farther from home consistently tend to align at higher levels.

In conclusion, we present a network-based segmentation of individual trajectories as a novel approach for understanding human mobility patterns across geographic extents. By examining modules within individual trajectories in relation to distance from home, we uncover the inflation phenomenon. This phenomenon is consistent across different demographics and regions, as confirmed by data from the US, Senegal, and Ivory Coast with an exponent around 0.6. However, compared to the US, the datasets from Senegal and Ivory Coast cover smaller geographic areas, resulting in reduced inflation beyond 100 km, likely due to boundary effects. Furthermore, we show the connection between the inflation law and the urban hierarchical structures. Urban hierarchies

facilitate mobility across different focal regions, culminating in the emergence of multiple modules in individual trajectories<sup>16</sup>. When people are far from home, their movement tends to be at higher hierarchical levels, leading to an increased geospatial extent of the modules. Beyond hierarchy, the urban environment is also associated with the distribution of population, infrastructure, and amenities. To analyze the impact of these features, we group modules based on the number of Points of Interest (POIs) at their destinations (see Fig.S12). Our analysis indicates that individuals visiting areas with higher POI density tend to remain within smaller module radii. Despite this, the overall trend of inflation persists, underscoring its robustness across varying urban contexts.

This study opens new perspectives on how home location influences human mobility within urban environments, with significant interdisciplinary applications<sup>17</sup>. In epidemic intervention, our findings can help refine epidemic modeling by incorporating differentiated mobility patterns based on distance from home, improving prediction accuracy and intervention effectiveness<sup>18</sup>. From a social equity standpoint, our results can help provide a more nuanced view of mobility segregation among racial groups, by considering neighborhood activities and movements beyond<sup>19</sup>. In urban resilience, this research can help cities tailor their response to emergencies and the restoration of essential services for residents and visitors at varying distances from their homes<sup>20</sup>.

## Methods

**Data.** Our analysis of human trajectories uses three datasets (see Supplementary Text): one from the US, one from Senegal, and another from the Ivory Coast. For data preprocessing, we aggregate closely situated or overlapping visited locations (e.g., adjacent rooms within the same building) into unique hexagons using the H3 geospatial indexing system<sup>15</sup> at resolution 12, where each hexagon has an edge length of approximately 9 meters. We identify users’ home locations as the hexagons they visited most frequently during nighttime hours (8 pm to 8 am).

**Extracting modules from trajectory networks.** For each user’s trajectory  $T = \{\theta_1, \dots, \theta_{i\dots}\}$ , where  $i$  is the sequence index of the stay point  $\theta_i$ , we construct the trajectory network  $G(T)$ , with each stay point as a node and consecutive trips between two stay points as edges. To characterize  $G(T)$  in geographic space, we define the edge weight  $W(T) = \{w(\theta_1, \theta_2), \dots, w(\theta_i, \theta_{i+1}), \dots\}$  and  $w(\theta_i, \theta_{i+1})$  is denoted as

$$w(\theta_i, \theta_{i+1}) = \log\left(\frac{\hat{d}}{d(\theta_i, \theta_{i+1})}\right) \quad (2)$$

where  $d(\theta_i, \theta_{i+1})$  is the spatial distance between stay points  $\theta_i$  and  $\theta_{i+1}$ , and  $\hat{d}$  corresponds to the maximum jump distance, constrained by the geographical size of each country ( $\hat{d} = 4,000\text{km}$  for the US, and  $\hat{d} = 1,000\text{km}$  for Senegal and Ivory Coast). Note that  $\hat{d} \geq d(\theta_i, \theta_{i+1})$  ensures that all weights remain non-negative after the log-transformation. Equation (2) assigns greater weight to shorter distances, employing an approach known as inverse distance weighting, grounded in Tobler’s first law of geography<sup>11</sup>, which posits that entities in close proximity are more likely to interact than those farther apart.

Subsequently, we apply a community detection method to detect modules in the weighted directed trajectory network  $G(T)$ . To ensure the geographical proximity of stay points within each module, we exclude outlier staying points located farther than half the module’s radius from its centroid. We also discard modules containing fewer than three locations. All characteristics of these identified modules are depicted in Fig. S2-S5.

**Delineating hierarchical levels in urban space.** To create a consistent spatial hierarchy across countries, we construct the hierarchical levels based on the H3 geospatial indexing system<sup>15</sup>. The H3 system divides space into discrete cells, each location is assigned a cell identifier, and lower resolutions are composed of higher resolutions. Here we consider resolutions from 1 to 7, with hexagon edge lengths varying from 418 kilometers to 1 kilometer. Starting from coarsest resolution  $\sigma = 1$ , given the spatial unit at level  $L$ , the hierarchy is constructed iteratively:

Step 1: Divide the spatial unit into cells at resolution  $\sigma + 1$ .

Step 2: Aggregate cells into new spatial units at level  $L - 1$  using community detection on collective flow matrix between cells, defining the radius  $R = \sqrt{S/\pi}$  for spatial units of size  $S$ .

The process continues through the two steps until the finest resolution,  $\sigma = 7$  is reached, producing a structured hierarchy where higher-level units encompass lower-level units (Fig. 2a and Fig. S16).

Given the generated spatial hierarchy, module  $c$  is assigned to level  $L_c = L$  if  $L$  is the smallest level where there exists a spatial unit satisfying  $\frac{N_c \cap N_L}{N_c} \geq 0.8$ , ensuring that at least 80% of the module’s stay points ( $N_c$ ) are covered by the spatial unit at level  $L$  ( $N_L$ ).



## References

1. Fotheringham, A. S. & O’Kelly, M. E. *Spatial Interaction Models: Formulations and Applications*, vol. 1 (Kluwer Academic Publishers, 1989).
2. Roy, J. R. & Thill, J. C. Spatial interaction modelling. *Papers in Regional Science* **83**, 339–361 (2004).
3. Mulligan, G. F., Partridge, M. D. & Carruthers, J. I. Central place theory and its reemergence in regional science. *The Annals of Regional Science* **48**, 405–431 (2012).
4. Brockmann, D., Hufnagel, L. & Geisel, T. The scaling laws of human travel. *Nature* **439**, 462–465 (2006).
5. Gonzalez, M. C., Hidalgo, C. A. & Barabasi, A.-L. Understanding individual human mobility patterns. *Nature* **453**, 779–782 (2008).
6. Batty, M. Hierarchy in cities and city systems. *Hierarchy in Natural and Social Sciences* 143–168 (2006).
7. Östh, J., Reggiani, A. & Schintler, L. A. Hierarchy, central place theory and computational modelling. In *Handbook on Entropy, Complexity and Spatial Dynamics*, 454–473 (Edward Elgar Publishing, 2021).
8. Alessandretti, L., Aslak, U. & Lehmann, S. The scales of human mobility. *Nature* **587**, 402–407 (2020).

9. Simini, F., González, M. C., Maritan, A. & Barabási, A.-L. A universal model for mobility and migration patterns. *Nature* **484**, 96–100 (2012).
10. Schläpfer, M. *et al.* The universal visitation law of human mobility. *Nature* **593**, 522–527 (2021).
11. Miller, H. J. Tobler’s first law and spatial analysis. *Annals of the Association of American Geographers* **94**, 284–289 (2004).
12. Blondel, V. D., Guillaume, J.-L., Lambiotte, R. & Lefebvre, E. Fast unfolding of communities in large networks. *Journal of Statistical Mechanics: Theory and Experiment* **2008**, P10008 (2008).
13. Bhat, C. R. & Koppelman, F. S. Activity-based modeling of travel demand. In *Handbook of Transportation Science*, 35–61 (Springer, 1999).
14. Miller, H. J. Activity-based analysis. *Handbook of Regional Science* 187–207 (2021).
15. H3: Uber’s hexagonal hierarchical spatial index. <https://www.uber.com/blog/h3/>. Accessed: 2023-09-01.
16. Cabrera-Arnau, C., Zhong, C., Batty, M., Silva, R. & Kang, S. M. Inferring urban polycentricity from the variability in human mobility patterns. *Scientific Reports* **13**, 5751 (2023).
17. Pappalardo, L., Manley, E., Sekara, V. & Alessandretti, L. Future directions in human mobility science. *Nature Computational Science* **3**, 588–600 (2023).

18. Belik, V., Geisel, T. & Brockmann, D. Natural human mobility patterns and spatial spread of infectious diseases. *Physical Review X* **1**, 011001 (2011).
19. Wang, Q., Phillips, N. E., Small, M. L. & Sampson, R. J. Urban mobility and neighborhood isolation in America's 50 largest cities. *Proceedings of the National Academy of Sciences* **115**, 7735–7740 (2018).
20. Haraguchi, M. *et al.* Human mobility data and analysis for urban resilience: A systematic review. *Environment and Planning B: Urban Analytics and City Science* **49**, 1507–1535 (2022).
21. Song, C., Koren, T., Wang, P. & Barabási, A.-L. Modelling the scaling properties of human mobility. *Nature Physics* **6**, 818–823 (2010).
22. Van Meeteren, M. & Poorthuis, A. Christaller and “big data”: recalibrating central place theory via the geoweb. *Urban Geography* **39**, 122–148 (2018).
23. Zipf, G. K. The P1P2/D hypothesis: On the intercity movement of persons. *American Sociological Review* **11**, 677–686 (1946).
24. Aslak, U. & Alessandretti, L. Infostop: Scalable stop-location detection in multi-user mobility data. *arXiv preprint arXiv:2003.14370* (2020).
25. Fresh, accurate places data built to power modern applications. <https://www.safegraph.com/products/places>. Accessed: 2024-11-21.
26. Clauset, A., Newman, M. E. & Moore, C. Finding community structure in very large networks. *Physical Review E—Statistical, Nonlinear, and Soft Matter Physics* **70**, 066111 (2004).

27. Cordasco, G. & Gargano, L. Community detection via semi-synchronous label propagation algorithms. In *2010 IEEE international workshop on: business applications of social network analysis (BASNA)*, 1–8 (IEEE, 2010).
28. Murtagh, F. & Contreras, P. Algorithms for hierarchical clustering: an overview. *Wiley Interdisciplinary Reviews: Data Mining and Knowledge Discovery* **2**, 86–97 (2012).
29. Alsbati, K., Ranka, S. & Singh, V. An efficient k-means clustering algorithm (1997).
30. Stouffer, S. A. Intervening opportunities: A theory relating mobility and distance. *American Sociological Review* **5**, 845–867 (1940).
31. Barbosa, H. *et al.* Human mobility: Models and applications. *Physics Reports* **734**, 1–74 (2018).
32. Barbosa, H., de Lima-Neto, F. B., Evsukoff, A. & Menezes, R. The effect of recency to human mobility. *EPJ Data Science* **4**, 1–14 (2015).

**Acknowledgments** We thank Jinzhu Yu for his assistance with pre-processing the mobility data and fruitful discussion. J.G. and L.Z. acknowledge the support of the US National Science Foundation under Grant No. 2047488. L.D. acknowledges the support of the National Natural Science Foundation of China (Grant No. 42422110) and the Fundamental Research Funds for the Central Universities, Peking University. Q.W. acknowledges the support of the US National Science Foundation under Grant No. 2125326.

**Author contributions** L.Z., L.D., Q.W., and J.G. conceived the project and designed the experiments; L.Z. and Q.W. collected and analyzed the data; L.Z., L.D., J.G., and C.S. carried out theoretical calculations and performed the experiments; all authors wrote and edited the manuscript.

**Competing interests** The authors declare no competing interests.

**Correspondence and requests for materials** should be addressed to J.G.

**Data and code availability** Data files and the code have been deposited in [https://github.com/1ucinezhong/Spatial\\_Inflation\\_Human\\_Mobility](https://github.com/1ucinezhong/Spatial_Inflation_Human_Mobility)

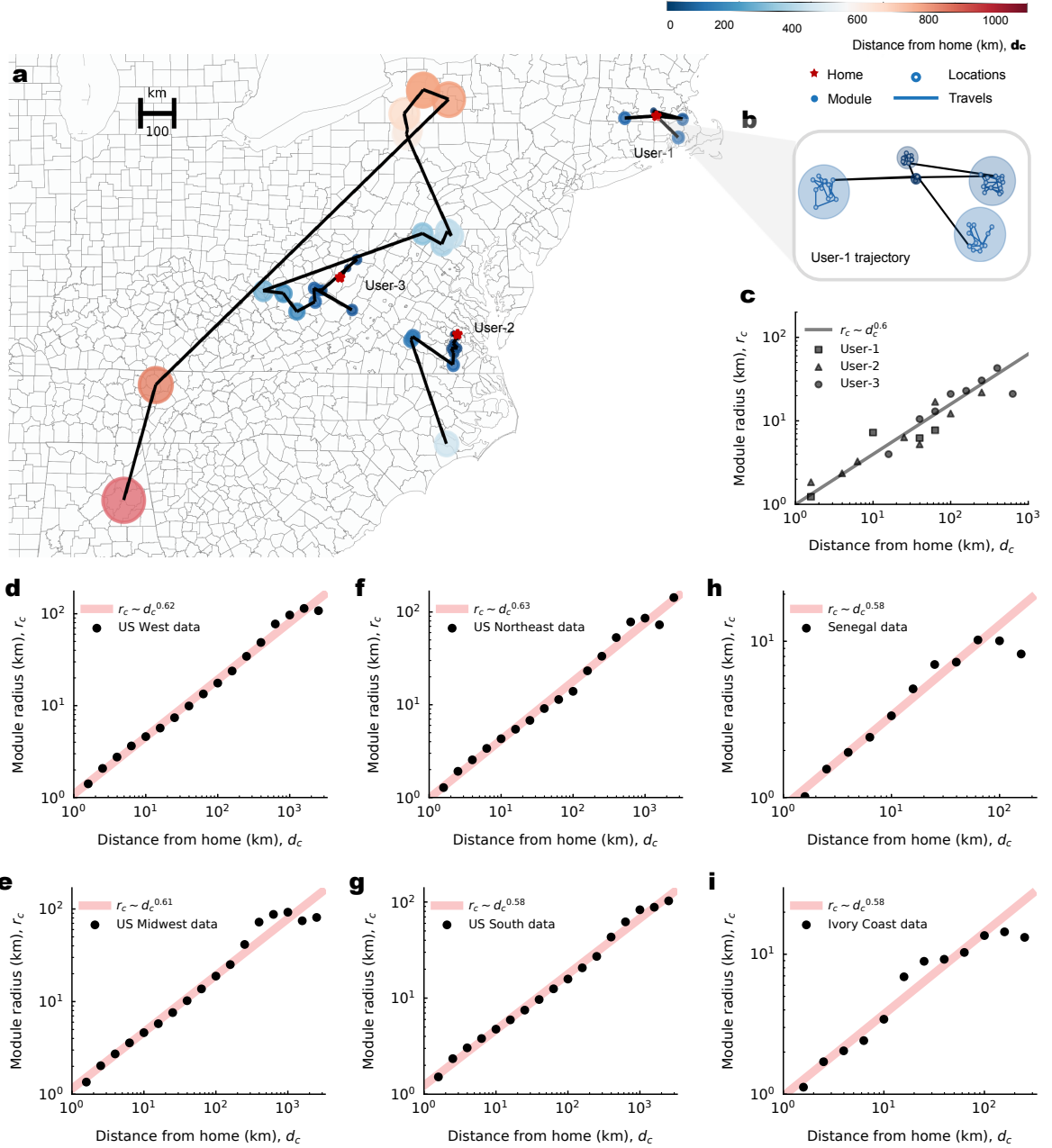


Figure 1: **The spatial inflation of modules.** (a) The spatial distribution of modules in anonymized cell phone users' trajectories. By representing trajectories as networks and applying the Louvain method, (b) the example trajectory network is divided into five modules, each encompassing spatially and topologically proximate locations. (c) Modules located far from home are in larger spatial coverage. By analyzing all U.S., Senegal, and Ivory Coast data, (d-i) module radius  $r_c$  increases with distance from home  $d_c$  in a power-law manner,  $r_c \sim d_c^\kappa$ . Specifically, for U.S. data in the West, Northeast, Midwest, and South regions, the value of  $\kappa$  is approximately  $0.61 \pm 0.03$ . For Senegal and Ivory Coast data,  $\kappa$  is approximately 0.58.

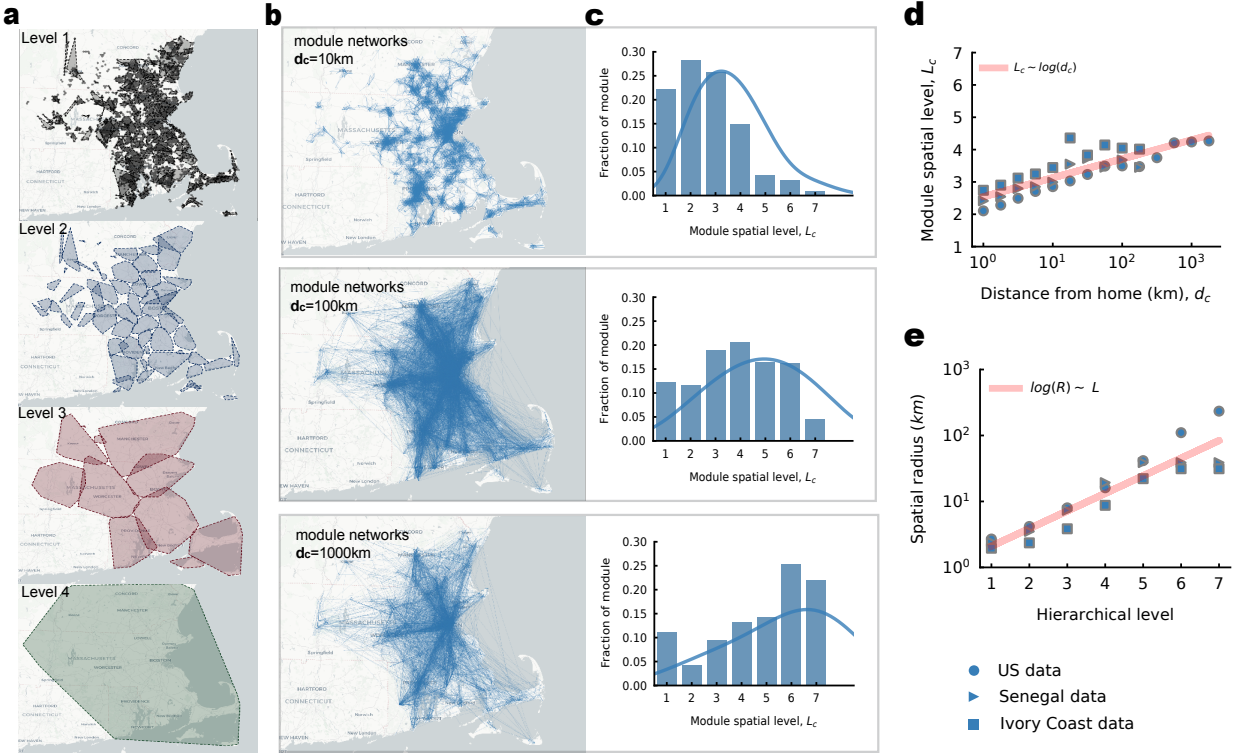


Figure 2: **Spatial hierarchical levels and inflation law.** With the destination Boston, Massachusetts as the example, (a) the urban environment is structured into four hierarchical levels  $L$ , with higher-level units covering lower-level units. We add the convex hull of aggregated H3 cells at each level to better illustrate the geographical extent. (b) Users' module networks at the destination with varying distances from home (e.g., 10km, 100km, 1000km). Modules that are at greater distances from home involve travel across higher hierarchical levels. We assign modules a specific level  $L_c$  if that hierarchical level unit covers the module at an 80% threshold. (c) The distribution of module levels  $L_c$ . By analyzing all U.S., Senegal, and Ivory Coast data, (d) the spatial levels of modules at varying distances from home follow  $L_c \sim \log(d_c)$ . (e) The spatial size of hierarchical levels follows  $\log(R) \sim L$ , leading to  $\log(R) \sim L = L_c \sim \log(d_c)$ .

## Contents

<b>1</b>	<b>Supplementary Note 1: Related Work</b>	<b>17</b>
<b>2</b>	<b>Supplementary Note 2: Mobility module</b>	<b>17</b>
<b>3</b>	<b>Supplementary Note 3: Spatial inflation robustness test</b>	<b>19</b>
<b>4</b>	<b>Supplementary Note 4: Connection with hierarchical levels.</b>	<b>21</b>



## 1 Supplementary Note 1: Related Work

Human mobility is significantly shaped by various factors, including individual self-preference, social and economic conditions, and the structure of the urban environment including the layout of streets, transportation networks, and the distribution of residential, commercial, and recreational areas. Among these, the role of "home" as a central location is particularly significant in shaping mobility patterns. As summarized in Table 1, from the perspective of individual activity demand, literature has demonstrated that individuals' activities tend to center their movements around their homes, with frequent returns to the anchor point<sup>13,14</sup>. This behavior, known as preferential return<sup>21</sup>, reflects the natural tendency for individuals to revisit familiar and recent places, particularly their homes. From the urban structural perspective, literature shows that cities are often organized in spatial hierarchies (Central Place Theory) that facilitate access to essential services and stores, which are typically located relatively close to residential areas<sup>3,7,22</sup>. This design enhances efficiency by minimizing travel distances for everyday activities. As a result, mobility flows and the number of visitors to different locations are observed to be inversely correlated with the distance from home<sup>1,2,10,23</sup>, with destinations closer to home encouraging more frequent trips. However, these studies primarily focus on specific spatial scales, leaving the influence of home location on human mobility across multiple spatial scales largely unexplored.

## 2 Supplementary Note 2: Mobility module

**Datasets** Table. 2 summarized three datasets we used: the US dataset, the Senegal dataset, and the Ivory Coast dataset.

**US dataset.** The U.S. dataset is from anonymized location-based service records provided by Cuebiq Inc. The originally provided dataset covers 42 million anonymized users from January to June 2020. All users opted-in to data collection for research purposes through a GDPR and CCPA compliant framework. To preserve privacy, the data provider obfuscates home locations in the dataset to the Census Block Group level. Employing the Infostop algorithm<sup>24</sup>, we processed each user's trajectories to identify stay points, resulting in a selection of roughly 2.1 million users with records spanning over thirty days. When exploring demographic characteristics, our investigation is grounded in data derived from the American Community Survey (ACS). These datasets are stratified by census block groups. We, therefore, integrated trajectories linked to census block

groups, offering insights into a spectrum of social, economic, and demographic across various regions in the U.S.

**Senegal dataset.** The Senegal dataset originates from anonymized call detail records, provided by the Data for Development Senegal Challenge in 2013. The dataset is divided into 25 distinct two-week intervals, containing approximately 44 million records linked to cell towers and attributed to around 300,000 randomly selected users.

**Ivory Coast dataset.** The Ivory Coast dataset originates fromn anonymized call detail records, provided by the Data for Development Ivory Coast Challenge, collected between December 2011 and April 2012. This dataset is divided into two-week periods and includes trajectories of 50,000 randomly sampled individuals over these intervals.

**POI dataset.** The Point of Interest (POI) data is provided by SafeGraph <sup>25</sup> and includes physical location details such as latitude, longitude, city, region, and postal code within the United States.

**Jump distance distribution.** We use the fundamental measures of jump distance to characterize human mobility in the three datasets. As shown in Fig. 3, the jump-distance distributions are approximated by  $P(\Delta r) \sim \Delta r^{-(1+\alpha)}$  where  $\alpha = 0.77, 1.22, 1.23$  respectively for United States, Senegal, and Ivory Coast data. When we closely examine travels that originate at distances from home ( $d$ ) of 10 km, 100 km, and 1000 km while excluding journeys back home, we observe a trend in Fig. 3d-f. As  $d$  increases, the distribution of jump lengths tends to have smaller exponents. Taking the United States data as an example, we find  $\alpha$  values of 0.89, 0.59, and 0.20 for  $d = 10, 100, 1000$  km, respectively. This same pattern is observed in the data from Senegal and Ivory Coast. This trend implies that when individuals travel far from home, they are more likely to initiate long-distance travel. It means that the power-law distribution of jump distances is not uniform for all users at any distance from home. The observations prompt us to explore the fair approach to segmenting human travel trajectories and to find the scaling at increasing distances from home.

**Mobility module: topological and spatial properties** Given our assumption that individual trajectories are impacted by interconnected urban structures, we utilize a network representation to

depict human trajectories, with nodes representing locations and edge weights symbolizing spatial distances, as described in the Methods section. We then extract modules from these human trajectory networks. Fig. 4 displays the distribution of the number of extracted modules, revealing that human networks exhibit segmentability with an average presence of multiple modules. Following segmentation, we proceed to analyze the topological and spatial properties of these modules.

**Module visitation.** We depict the visitation frequency of modules in Fig. 5. The visitation frequency decays with module distance  $d_c$ , indicating that humans are less likely to visit modules far from home.

**Module topological size.** We use the number of nodes and edges with network modules to characterize the topological size. As shown in Fig. 6 and Fig. 7, we use the home as the reference point to identify module location  $d_c$ . As the module distance from home,  $d_c$  increases, both the number of nodes (representing unique locations within modules) and the number of edges (representing travels within modules) decrease. In terms of network topology, module sizes tend to become smaller when far from home.

**Module spatial size.** For module spatial size, we use the radius  $r_c$ , that is, the average distance from locations to the module centroid to measure the module size. We find that module radius sub-linearly increases with module distance to home in logarithmic scales,  $r_c \sim d_c^k$ . To guarantee the finding is objective and systematic, we also use the area size ( $A_c$ ) of the convex hull formed by visited locations within modules to characterize module size. Fig. 8 shows that in the United States, Senegal, and Ivory Coast data, the modules' convex hull size ( $A_c$ ) correlates with  $d_c$  in logarithmic scales,  $A_c \sim d_c^{k'}$ . It again justifies that as humans venture farther away from their homes, the size of modules increases exponentially with home serving as the reference point.

### 3 Supplementary Note 3: Spatial inflation robustness test

**Different community detection algorithms** We test the trend of module radius increasing with distance from home using different community detection algorithms, i.e., Clauset-Newman-Moore greedy modularity maximization<sup>26</sup>, Label propagation community detection<sup>27</sup>, Hierarchical clus-

tering<sup>28</sup>, and K-means clustering<sup>29</sup>. As shown in Fig. 9, the trends, that is, the increase in module radius with distance from home, remain consistent across most community detection algorithms. For the Greedy Modularity algorithm, Hierarchical clustering, and K-means clustering, the exponent  $\kappa$  is close to the inflation law found in the manuscript using the Louvain method, near 0.6. However, for the Label Propagation algorithm, which is suitable only for unweighted networks, the exponent  $\kappa$  is significantly smaller.

**Different edge weights** To test whether different definitions of edge weight impact the module detection and observed inflation mobility pattern, we also proposed two alternative definitions of edge weight. Compared with the one used in the manuscript, the definition  $w(\theta_i, \theta_j) = \hat{d} - d(\theta_i, \theta_j)$  in Fig. 10b yields an inflation law with the same exponent of approximately  $\kappa = 0.6$ . Though the second definition  $w(\theta_i, \theta_j) = \frac{\hat{d}}{d(\theta_i, \theta_j)}$  (Fig. 10c) causes the module radius to increase with distance from the home, it results in a varying exponent of  $\kappa = 0.16$ . This difference arises because, in the Louvain method of cluster detection, the weights are normalized by the sum of all edges' weights, and connected edges with closer weights are more likely to belong to the same module. Definition in Fig. 10c exaggerates the difference between larger and smaller weights, resulting in modules with smaller spatial sizes.

**Different regions** To ensure the universality of inflation mobility pattern across different subpopulations, we categorize users' trajectories based on which states their home locations belong to in the United States data, as shown in Fig. 11 and Fig. 12. We exclude states with fewer than 1000 users. Interestingly, individuals from different states exhibit consistent inflation patterns. While the exponent  $\kappa$  varies from state to state, it consistently keeps around a value of approximately 0.60.

**Different demographics** We also categorize the users' trajectories according to their home locations' demographic attributes (e.g., age, gender, race and ethnicity, and poverty level) to inspect the module size for each group of individuals in Fig. 13. Individuals with different demographic features show no significant difference for a relationship,  $r_c \sim d_c^\kappa$ . This means that spatial inflation is consistent across user groups living in regions with different demographic attributes.

**Destinations with varying POI density** To explore how the features of destinations, such as the number of Points of Interest (POIs), affect the inflation law, we categorize modules based on the number of POIs at destinations. The destination POI density is measured as the total POI

count within a fixed 10-square-kilometer area. Nationally, POIs follow a long-tail distribution, as depicted in Fig. 14a. Our analysis reveals that the module radius generally expands with increasing distance in Fig. 14b. However, at destinations with a high POI count, the module radius tends to be smaller when  $d_c > 20$  km. A likely explanation is that in areas with an abundance of resources (top 10% of POIs), short-distance exploration typically meets human needs. Conversely, in areas with fewer resources (bottom 10% of POIs), longer distances are necessary for exploration. These findings indicate that module sizes farther from home are more likely to be influenced by destinations' resource abundance. Despite this, the inflation tendency consistently holds.

**Data imbalance** To test the impact of data imbalance on our findings, that is, whether having more data points near home leads to a smaller radius, we applied the down-sampling techniques to disproportionately sample subsets of stay points closer to home in individual trajectories. We randomly selected half of the records from the original dataset within a 100 km radius of the home. As depicted in Fig. 15, reducing the number of records near home slightly increases the radii in that area and decreases the exponent  $\kappa$ . While minor effects are observed, the overall inflation pattern relative to distance from home remains robust when we down-sampling the data points.

**COVID-19 lockdown period** The COVID-19 lockdown is known to have altered people's mobility patterns, with the most notable changes observed in U.S. datasets being a decrease in the frequency of travel. However, despite these changes, we consistently find that the spatial inflation phenomenon, where the module radii increase with the module distance ( $r_c \sim d_c^\kappa$ ), remains unchanged for both the pre-lockdown and post-lockdown periods, as illustrated in Fig. 16.

#### 4 Supplementary Note 4: Connection with hierarchical levels.

**Administrative hierarchical levels** Besides testing the connection of mobility modules with our defined hierarchical levels, we also test it on the administrative hierarchy defined by the US Census Bureau: region ( $L = 4$ ), state ( $L = 3$ ), county ( $L = 2$ ), and country division ( $L = 1$ ). As shown in Fig. 17a, the spatial radius increases with the hierarchical level, following the relationship  $\text{Log}(R) \sim L$ . We then tested the overlap of individual modules with these administrative levels. For modules farther from home, individual mobility patterns tend to align with higher hierarchical levels in Fig. 17b. The results on administrative levels are consistent with the results obtained using our constructed hierarchical levels (Fig. 18).

1. Fotheringham, A. S. & O’Kelly, M. E. *Spatial Interaction Models: Formulations and Applications*, vol. 1 (Kluwer Academic Publishers, 1989).
2. Roy, J. R. & Thill, J. C. Spatial interaction modelling. *Papers in Regional Science* **83**, 339–361 (2004).
3. Mulligan, G. F., Partridge, M. D. & Carruthers, J. I. Central place theory and its reemergence in regional science. *The Annals of Regional Science* **48**, 405–431 (2012).
4. Brockmann, D., Hufnagel, L. & Geisel, T. The scaling laws of human travel. *Nature* **439**, 462–465 (2006).
5. Gonzalez, M. C., Hidalgo, C. A. & Barabasi, A.-L. Understanding individual human mobility patterns. *Nature* **453**, 779–782 (2008).
6. Batty, M. Hierarchy in cities and city systems. *Hierarchy in Natural and Social Sciences* 143–168 (2006).
7. Östh, J., Reggiani, A. & Schintler, L. A. Hierarchy, central place theory and computational modelling. In *Handbook on Entropy, Complexity and Spatial Dynamics*, 454–473 (Edward Elgar Publishing, 2021).
8. Alessandretti, L., Aslak, U. & Lehmann, S. The scales of human mobility. *Nature* **587**, 402–407 (2020).
9. Simini, F., González, M. C., Maritan, A. & Barabási, A.-L. A universal model for mobility and migration patterns. *Nature* **484**, 96–100 (2012).
10. Schläpfer, M. *et al.* The universal visitation law of human mobility. *Nature* **593**, 522–527 (2021).
11. Miller, H. J. Tobler’s first law and spatial analysis. *Annals of the Association of American Geographers* **94**, 284–289 (2004).
12. Blondel, V. D., Guillaume, J.-L., Lambiotte, R. & Lefebvre, E. Fast unfolding of communities in large networks. *Journal of Statistical Mechanics: Theory and Experiment* **2008**, P10008 (2008).
13. Bhat, C. R. & Koppelman, F. S. Activity-based modeling of travel demand. In *Handbook of Transportation Science*, 35–61 (Springer, 1999).

14. Miller, H. J. Activity-based analysis. *Handbook of Regional Science* 187–207 (2021).
15. H3: Uber’s hexagonal hierarchical spatial index. <https://www.uber.com/blog/h3/>. Accessed: 2023-09-01.
16. Cabrera-Arnau, C., Zhong, C., Batty, M., Silva, R. & Kang, S. M. Inferring urban polycentricity from the variability in human mobility patterns. *Scientific Reports* **13**, 5751 (2023).
17. Pappalardo, L., Manley, E., Sekara, V. & Alessandretti, L. Future directions in human mobility science. *Nature Computational Science* **3**, 588–600 (2023).
18. Belik, V., Geisel, T. & Brockmann, D. Natural human mobility patterns and spatial spread of infectious diseases. *Physical Review X* **1**, 011001 (2011).
19. Wang, Q., Phillips, N. E., Small, M. L. & Sampson, R. J. Urban mobility and neighborhood isolation in America’s 50 largest cities. *Proceedings of the National Academy of Sciences* **115**, 7735–7740 (2018).
20. Haraguchi, M. *et al.* Human mobility data and analysis for urban resilience: A systematic review. *Environment and Planning B: Urban Analytics and City Science* **49**, 1507–1535 (2022).
21. Song, C., Koren, T., Wang, P. & Barabási, A.-L. Modelling the scaling properties of human mobility. *Nature Physics* **6**, 818–823 (2010).
22. Van Meeteren, M. & Poorthuis, A. Christaller and “big data”: recalibrating central place theory via the geoweb. *Urban Geography* **39**, 122–148 (2018).
23. Zipf, G. K. The P1P2/D hypothesis: On the intercity movement of persons. *American Sociological Review* **11**, 677–686 (1946).
24. Aslak, U. & Alessandretti, L. Infostop: Scalable stop-location detection in multi-user mobility data. *arXiv preprint arXiv:2003.14370* (2020).
25. Fresh, accurate places data built to power modern applications. <https://www.safegraph.com/products/places>. Accessed: 2024-11-21.
26. Clauset, A., Newman, M. E. & Moore, C. Finding community structure in very large networks. *Physical Review E—Statistical, Nonlinear, and Soft Matter Physics* **70**, 066111 (2004).

27. Cordasco, G. & Gargano, L. Community detection via semi-synchronous label propagation algorithms. In *2010 IEEE international workshop on: business applications of social network analysis (BASNA)*, 1–8 (IEEE, 2010).
28. Murtagh, F. & Contreras, P. Algorithms for hierarchical clustering: an overview. *Wiley Interdisciplinary Reviews: Data Mining and Knowledge Discovery* **2**, 86–97 (2012).
29. Alsabti, K., Ranka, S. & Singh, V. An efficient k-means clustering algorithm (1997).
30. Stouffer, S. A. Intervening opportunities: A theory relating mobility and distance. *American Sociological Review* **5**, 845–867 (1940).
31. Barbosa, H. *et al.* Human mobility: Models and applications. *Physics Reports* **734**, 1–74 (2018).
32. Barbosa, H., de Lima-Neto, F. B., Evsukoff, A. & Menezes, R. The effect of recency to human mobility. *EPJ Data Science* **4**, 1–14 (2015).



[h!]

Aspects	Literature in geography, regional science and transportation science	Spatial scales	Human mobility pattern
Population mobility	Gravity model <sup>1,2,23</sup> / Intervening opportunity model <sup>30</sup> , Radiation model <sup>9,31</sup>	Inter-city / Intra-city	Distance Decay: Mobility flow is negatively correlated with distance or opportunities between two locations
Individual mobility	Activity-based models (Characterize home-based and non-home-based trips) <sup>13,14</sup>	Intra-city	Preferential Return <sup>21</sup> : Individuals have a preference to return frequently-visited locations like home; Recency <sup>32</sup> : Individuals have a preference to return recently-visited locations
Urban Structure	Central Place Theory (Settlements are organized in spatial hierarchies) <sup>3,7,22</sup>	Inter-city / Region	Transportation costs determine the size of the space division; low level central locations provide functions with high frequency and short distance access.

Table 1: Summary of literature in human mobility pattern.

[t!]

Table 2: Statistics of trajectory data. Here "m" stands for one million.

	Time period	Total users (m)	Total records (m)	Records		Days	
				mean	median	mean	median
US (processed)	2020-01 to 2020-06	2.1	599	284	254	45	40
Senegal	2013-01 to 2013-12	0.32	44	138	86	12	13
Ivory coast	2011-12 to 2012-04	0.05	0.508	101	48	9	11

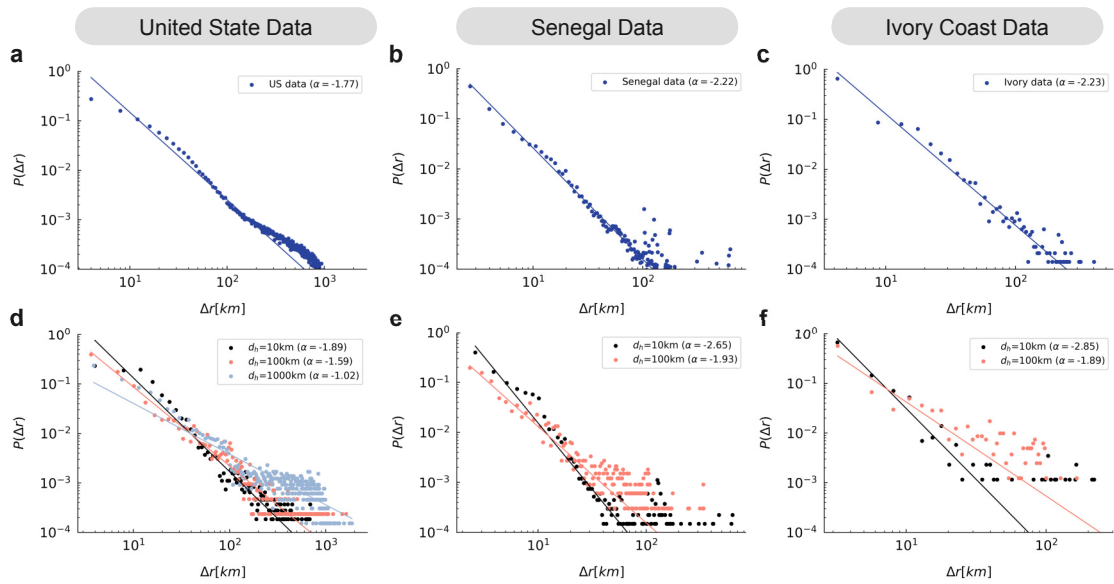


Figure 3: **Jump distance distribution for the United States, Senegal, and Ivory Coast data.** (a,b,c) Jump distance  $\Delta r$ , follows a power-law distribution characterized by  $P(\Delta r) \sim \Delta r^{-(1+\alpha)}$ . (d,e,f) Jump distance distribution if travel initiate at  $d_h = 10, 100, 1000$  km, respectively, with the exponent  $\alpha$  becoming smaller.

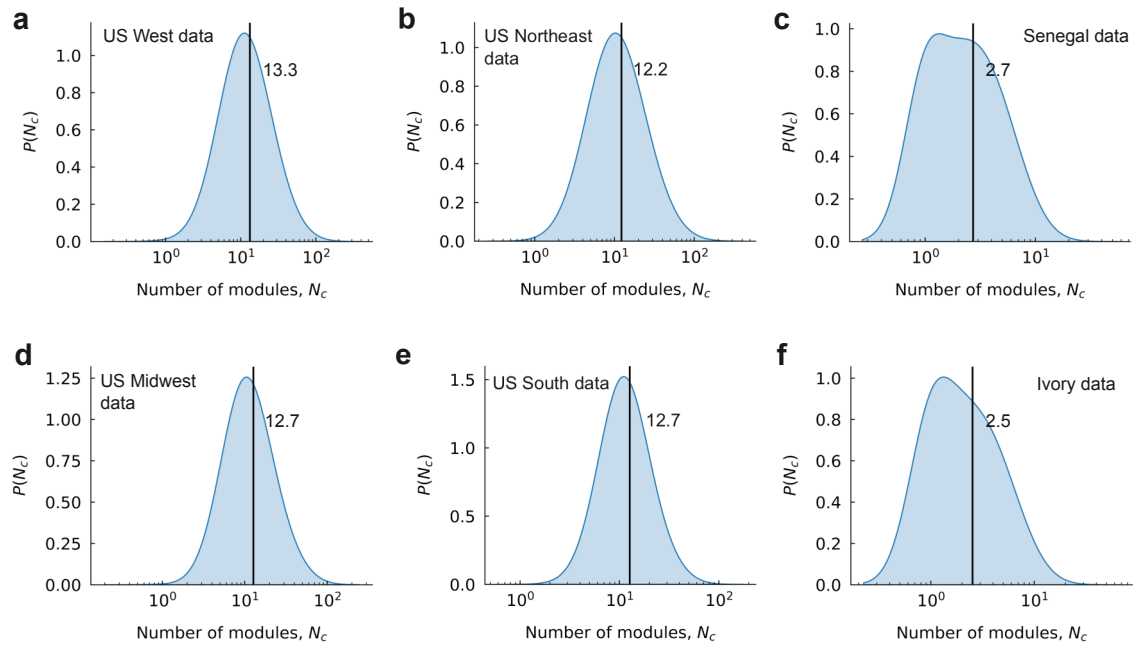


Figure 4: **Module counts within user trajectory networks for data from the United States, Senegal, and Ivory Coast data.** Users in the United States dataset typically have an average of twelve modules. As for the Senegal and Ivory Coast data, which are Detail Records with lower resolution, users typically have an average of three modules. Human trajectory networks exhibit segmentability.

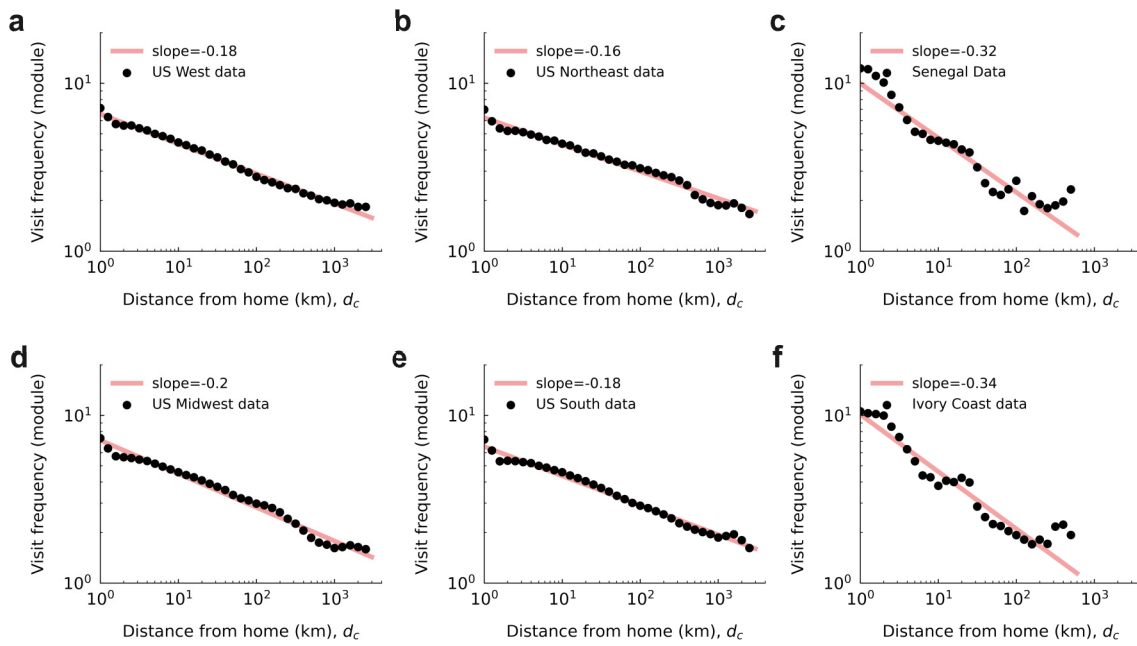


Figure 5: **Visitation frequency of module for data from the United States, Senegal, and Ivory Coast data.** As the module distance increases, the visitation frequency decreases.

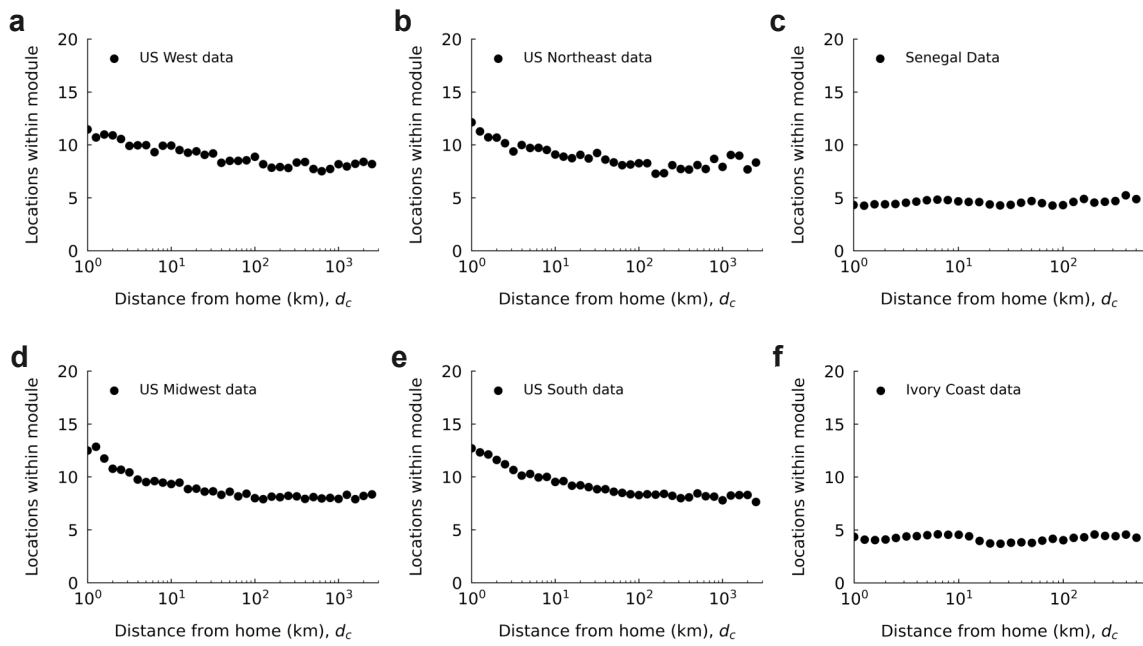


Figure 6: **Locations (Nodes) within modules for data from the United States, Senegal, and Ivory Coast data.** As the module distance increases, the counts of locations within modules slightly decrease. locations count decreases.

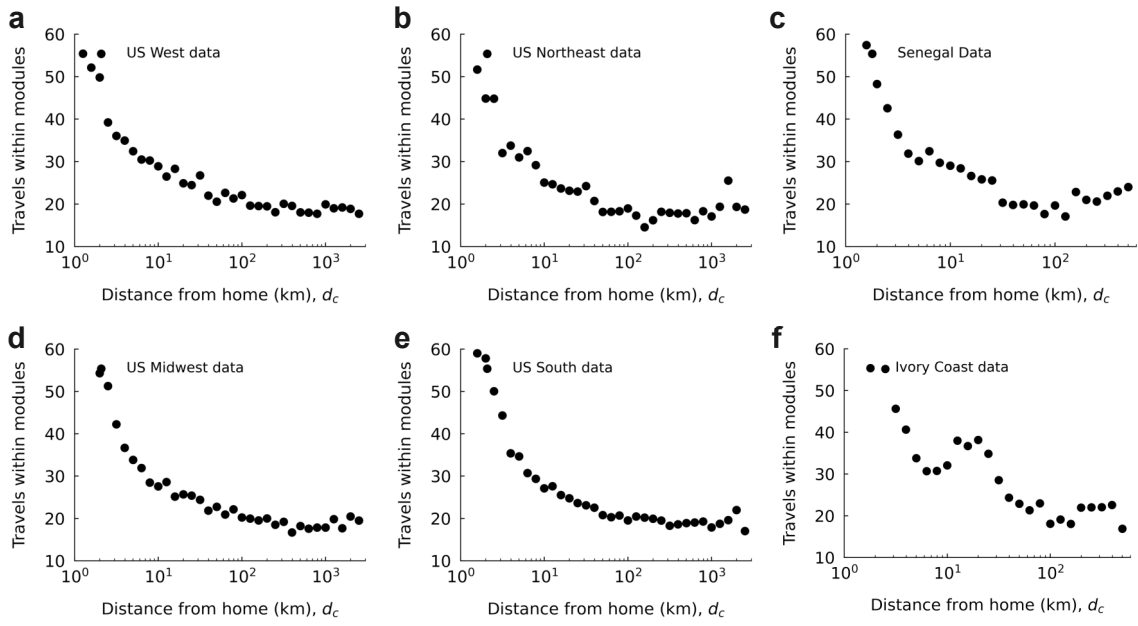


Figure 7: **Travels (Edges) within modules for data from the United States, Senegal, and Ivory Coast data.** As the module distance increases, the counts of travels within modules decrease.

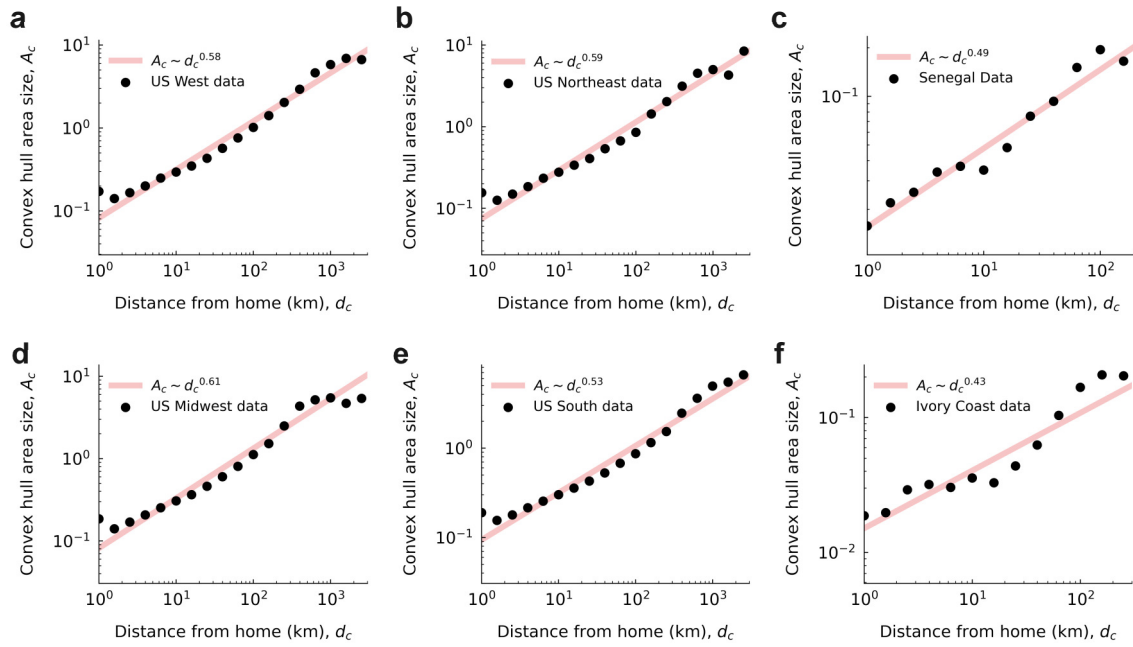


Figure 8: **The spatial inflation of modules regarding convex hull area size.** Module convex hull area size,  $A_c$ , increases sub-linearly with its distance from home  $d_c$ . The exponent is around 0.55 for the U.S. data, 0.52 for the Senegal data, and 0.44 for the Ivory Coast data.



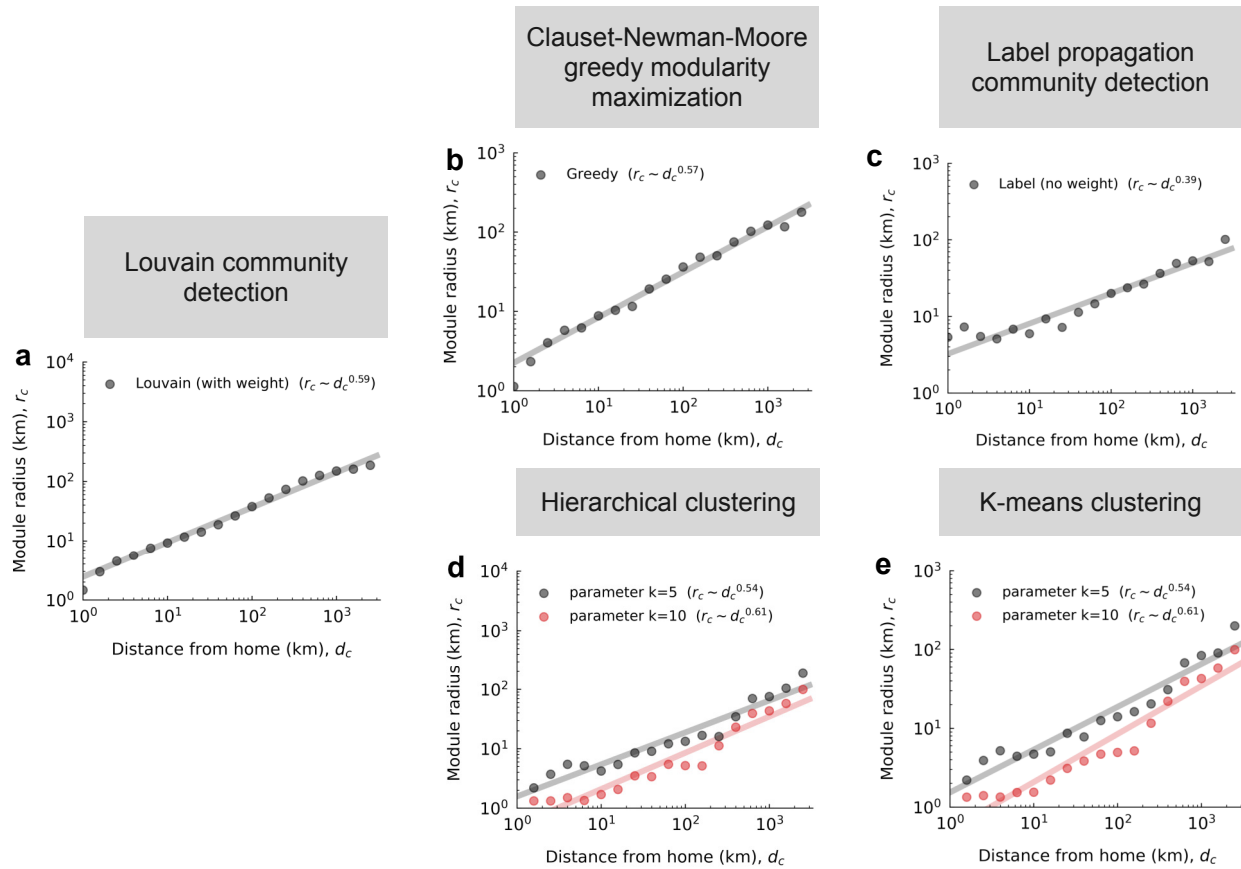


Figure 9: **Module radius versus distance from home, using different community detection algorithms.** (a) Louvain community detection (used in the manuscript). (b) Clauset-Newman-Moore greedy modularity maximization. (c) Label propagation community detection, which only suits the unweighted network. (d) Hierarchical clustering, which requires the preset number of clusters,  $k$ . (e) K-means clustering, which requires the preset number of clusters,  $k$ .

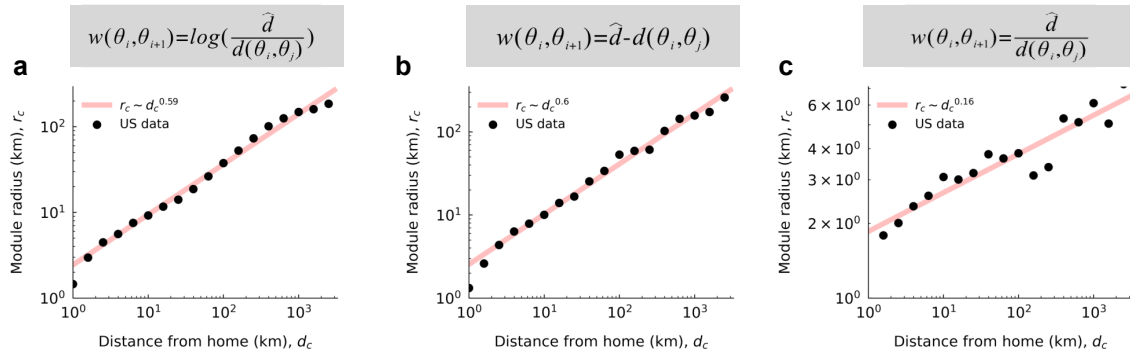


Figure 10: **Module radius versus distance from home, under different definitions of edge weight.** (a) Edge weight is defined by  $w(\theta_i, \theta_j) = \log\left(\frac{\hat{d}}{d(\theta_i, \theta_j)}\right)$  (definition in manuscript). (b) Edge weight is defined by  $w(\theta_i, \theta_j) = \hat{d} - d(\theta_i, \theta_j)$ . (c) Edge weight is defined by  $w(\theta_i, \theta_j) = \frac{\hat{d}}{d(\theta_i, \theta_j)}$ .

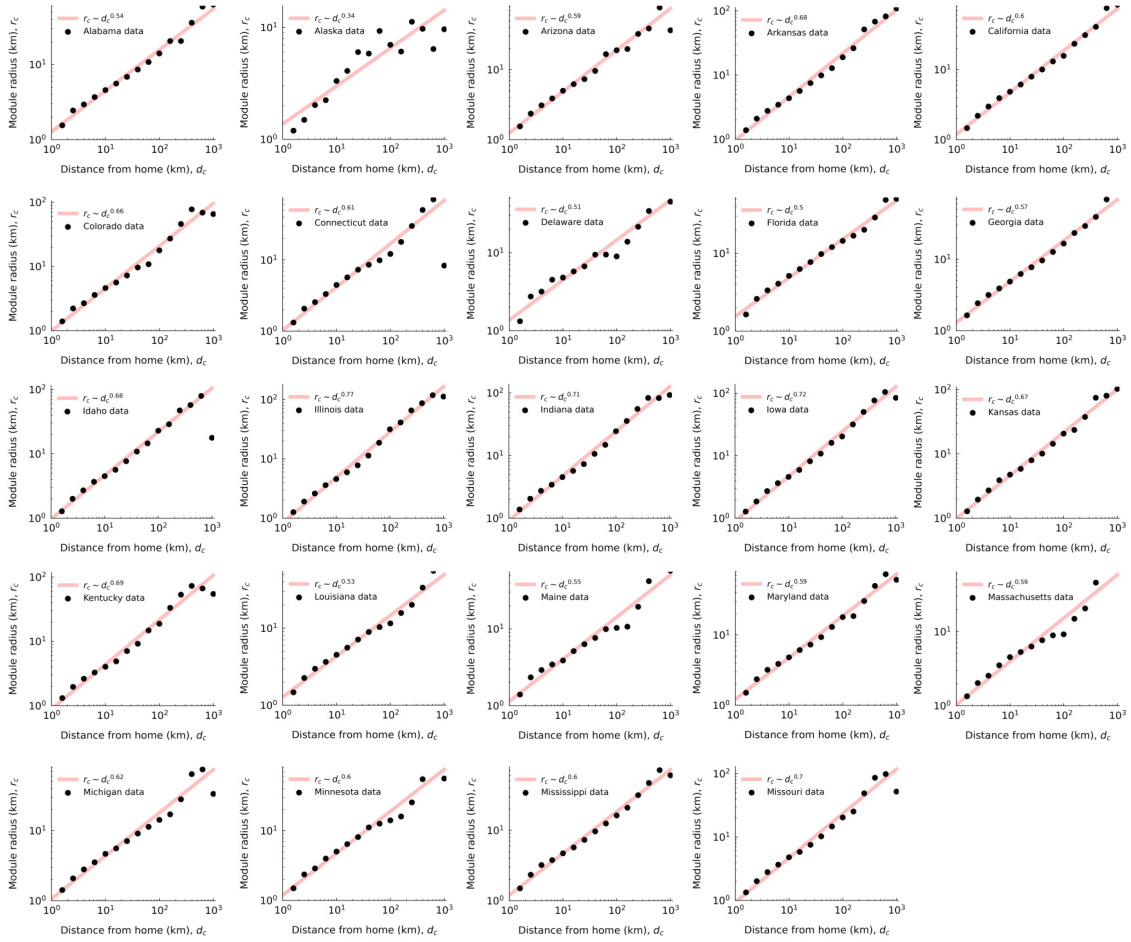


Figure 11: **Part-1-Module radius versus distance from home, for populations in different states.** By categorizing users based on the states of their home locations, the spatial inflation of the module remains consistent.

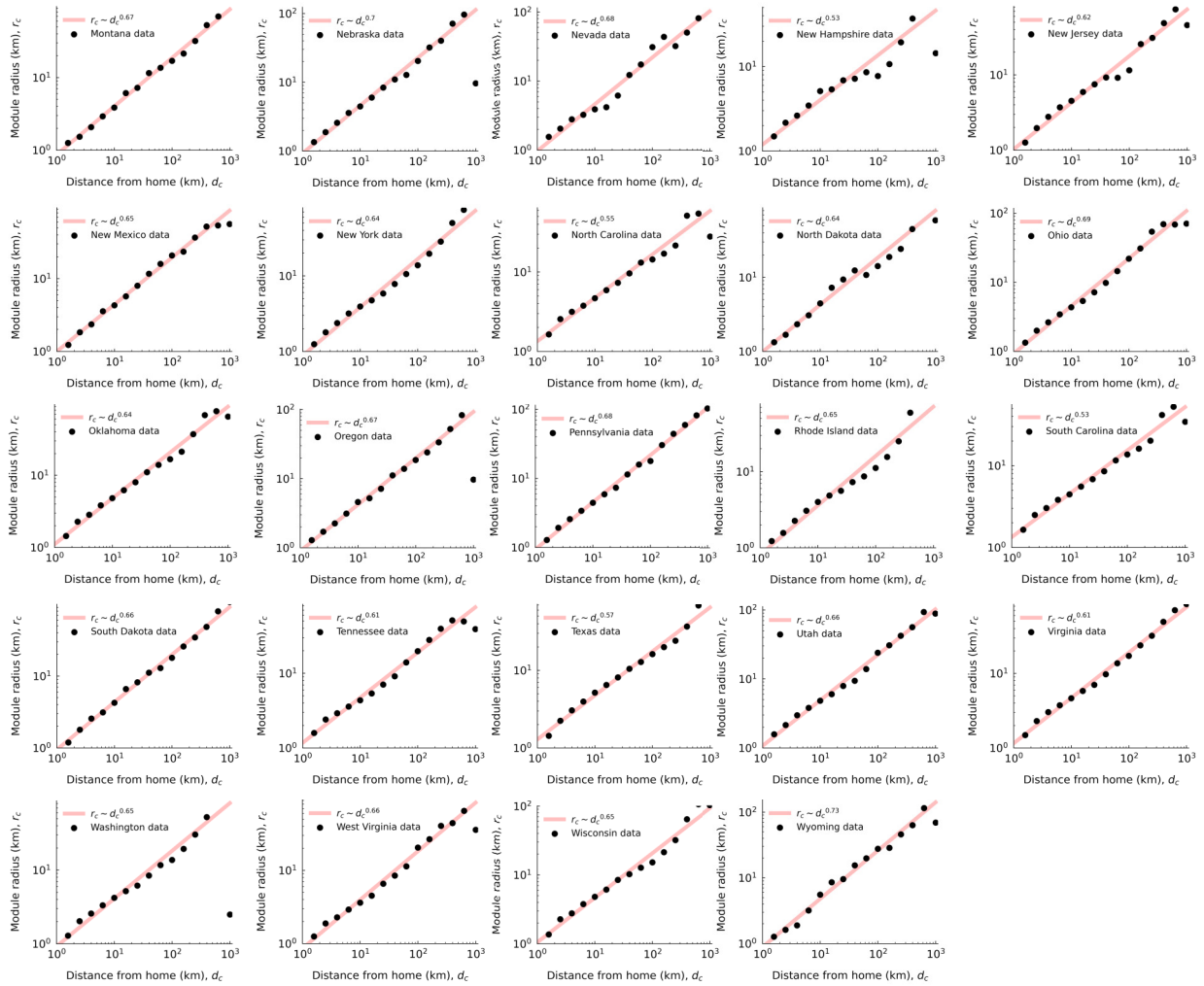


Figure 12: **Part-2-Module radius versus distance from home, for populations in different states.** By categorizing users based on the states of their home locations, the spatial inflation of the module remains consistent.

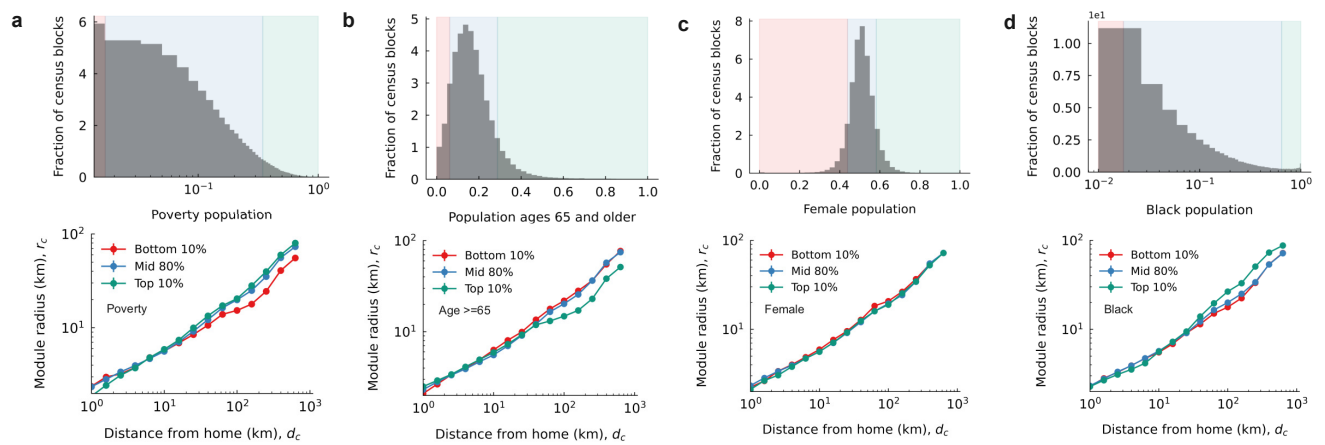


Figure 13: **Module radius versus distance from home, for populations in different demographic attributes.** By categorizing users based on the proportions of the poverty population in their home locations (a), the elderly population (age 65 and older) (b), the female population (c), and the black population (d), the spatial inflation of module remains consistent across various user groups.

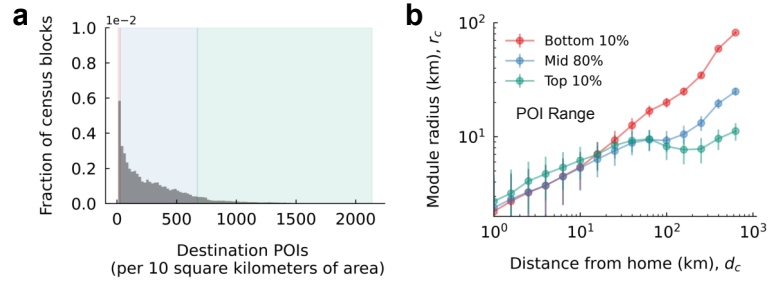


Figure 14: **Module radius versus distance from home, in destinations with different POI densities.** (a) Distribution of the number of Points of Interest (POIs) in destinations. (b) When categorizing destinations according to the number of points of interest (POIs), module radius versus distance from home.

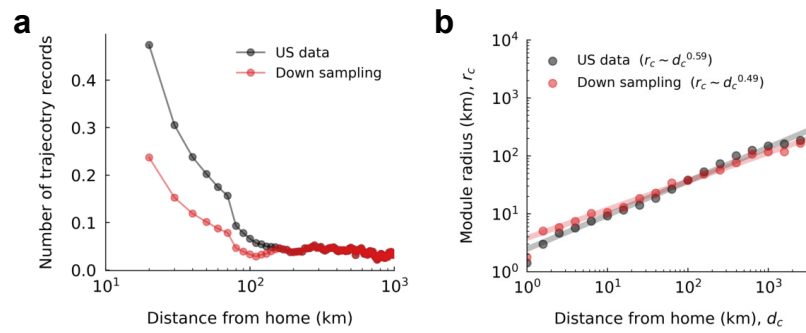


Figure 15: **Module radius versus distance from home, when down-sampling near-home trajectory records.** (a) Proportion of trajectory records after down-sampling compared to the original dataset. (b) Module radius versus distance from home under the down-sampling strategy.

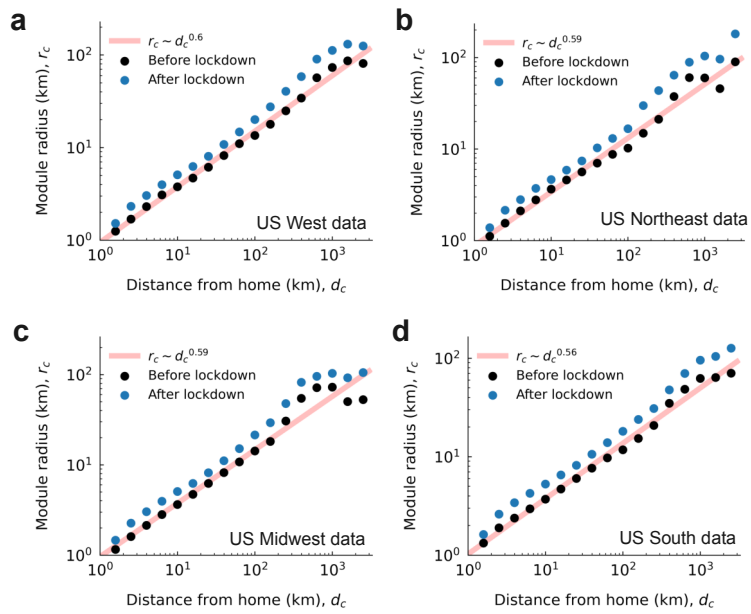


Figure 16: **Module radius versus distance from home, during before-lockdown period and after-lockdown period.** We set March 11 as the date to split the U.S. data into the before-lockdown period and after-lockdown period.



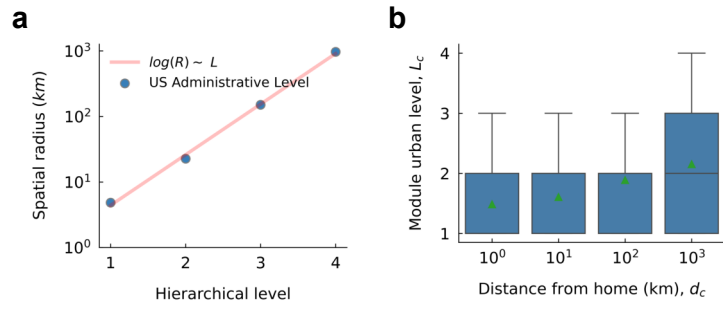


Figure 17: **Administrative hierarchical levels and mobility modules.** (a) Spatial radius of administrative hierarchy levels as defined by the US Census Bureau: region ( $L = 4$ ), state ( $L = 3$ ), county ( $L = 2$ ), and county division ( $L = 1$ ). (b) Spatial levels of mobility modules at varying distances from home.

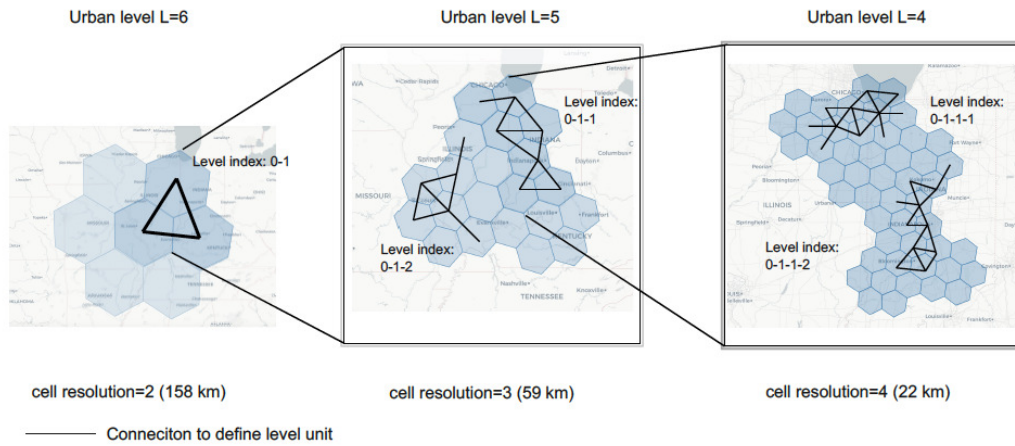


Figure 18: **Illustration of delineating hierarchical levels.** Using cell resolutions ranging from 2 to 4 as an example, the spatial unit at resolution 2, identified by the level index "0-1," is subdivided into smaller sub-spatial units at the higher resolution of 3. These sub-spatial units are assigned lower-level indices, such as "0-1-1" and "0-1-2". This process is applied iteratively across resolutions, progressing from resolution 1 to resolution 7, to establish a hierarchical structure from level 7 to level 1. The figure is created for illustrative purposes only and does not represent actual data.